

The Effect of Ni Doping on the AC Conductivity and Dielectric Properties of Fe-Doped TiO₂

Marwa Belhaj^{1,3*}, TA Abdel-Basset^{1,2}, Mosa Aelsehli⁴ and Ali H Bashal⁴

¹Department of Physics, Taibah University, Yanbu, Saudi Arabia

²Department of Physics, Fayoum University, Fayoum, Egypt

³Nanomisene Lab LR16CRMN01, Center of Research on Microelectronics and Nanotechnology of Sousse, Technopark of Sousse, Sahloul Sousse, Tunisia

⁴Department of Chemistry, Taibah University, Yanbu, Saudi Arabia

*Corresponding author: Marwa Belhaj, Department of Physics, Faculty of Science, Taibah University, Yanbu, Saudi Arabia; E-mail: marwabelhaj2@gmail.com

Received date: September 21, 2021; Accepted date: October 06, 2021; Published date: October 13, 2021

Abstract

Owing to its peculiar physical properties, Titanium Dioxide (TiO₂) has found various applications and been an interactive material for research in the field of semiconductor physics. To study the crystallographic nature of prepared Fe/TiO₂ and Ni-Fe/TiO₂, X-ray Diffraction (XRD) study was done. The result shows that both pure and doped TiO₂ samples were anatase phase with the absence of diffraction peaks of Ni or Fe. The Scanning Electron Microscopy (SEM) images revealed that the particle morphology was altered by dopants incorporation which acted as nucleation sites. The dielectric properties and electrical conductivity for TiO₂ and TiO₂ loaded Fe, Ni and Ni-Fe composition within the temperature range 25°C-110°C and over the frequency range (100 Hz-0.3 MHz) were also carried out. The values of dielectric constant and dielectric loss decrease with increasing frequency. The dielectric permittivity for Fe/TiO₂ exhibits relatively lower dielectric constant than Ni-Fe/TiO₂. A relaxation peak has been recognized and shifted to higher frequency with increasing temperature. The ac conductivity was found to increase with frequency which could be related to the hopping conduction process. The activation energy E_a for Fe/TiO₂ was higher than Ni-Fe/TiO₂ and decreased with increasing frequency.

Keywords: Fe doped TiO₂; Ni-Fe doped TiO₂; AC conductivity; Dielectric properties; Activation energy

Introduction

The development of high-energy-density storage devices and capacitors, recently, has motivated many investigators to find a new dielectric material [1]. With the intention of making valuable dielectric materials, the materials should have the following features; low dielectric loss (<10⁻¹), high dielectric constant (>10³), and dielectric properties nearly independent of frequency and temperature. Dielectric materials such as BaTiO₃ [2], NiO [3], and CuO [4] have been proposed in the literature however these types of materials did not meet all these four features. Therefore, finding a new type of material is valued. Titanium dioxide TiO₂ is a member of the

transition metal oxides family [5]. It exists in three different phases namely rutile, brookite and anatase. It is found that anatase has a lower dielectric constant than the rutile phase of TiO₂ [6].

Among all the inorganic oxides (TiO₂) is a well-known semiconductor due to its distinguished optoelectronic and electrical properties for application in sensors and memory devices. Furthermore, TiO₂ has rich sources and improved chemical stability compared to other materials such as SrTiO₃ and CaCu₃Ti₄O₁₂ [1]. Because of its high dielectric constant and high breakdown strength, TiO₂ serves as a good insulator and had been found suitable for wide application in the field of electronic [7]. It is highly useful for the fabrication of capacitors used in microelectronics devices, electronic memories and in optical filters [8,9]. The low loss factors and high dielectric permittivity of TiO₂ over an ample frequency range are always of immense attention [10]. Furthermore, the dielectric and electric properties of TiO₂ could be altered easily by applying different temperatures and in the presence of intrinsic impurities and dopants. The effects of metal ion doping such as Nb, Ta, Al, Ca, Y, and Ba on the properties of TiO₂ have been investigated in the literature normously [11-13]. However, few works investigating the effect of co-doping metal ion on the dielectric properties of TiO₂ can be reported.

It has been found that a mono-metal-doped TiO₂ has a diverse dielectric property compared to the bimetallic-doped TiO₂ such as (In +Nb)-co-doped rutile titanium dioxide. The former material displays a high dielectric constant, low dielectric loss, and slight temperature dependence over the temperature range of 80-450 K [14]. Therefore, it is useful to find out new co-doped TiO₂ dielectric materials in order to improve the dielectric properties of TiO₂.

In this work, we produced a new (Ni-Fe)-co-doped TiO₂ system and compared it with Fe doped TiO₂ which was also synthesized by incipient wet impregnation method. We investigated the effect of Fe doped TiO₂ and co-doped (Ni-Fe) TiO₂ on structural properties, ac conductivity, dielectric properties, and the activation energy of TiO₂.

Experimental Methods

Materials

The precursor used to synthesize the nano-composites was nickel chloride, purchased from "Asaggaf-Pharma-Holyland" (production of KSA), Iron chloride (98%), CAS Number 7758-94-3, and titanium (IV) oxide, anatase (≥ 99% trace metals basis), CAS number 1317-70-0, which were obtained from Sigma-Aldrich (USA). All aqueous solutions in the synthesis were prepared using deionized water. All chemicals were used without further purification.

Composites preparation

Co-doped TiO₂ composite (Ni-Fe/TiO₂) and single doped TiO₂ (Ni/TiO₂ and Fe/TiO₂) composites were prepared by the incipient wet impregnation method following the procedure described earlier [15]. In brief, the suspension of TiO₂ was stirred at room temperature for around 10 min to confirm the full bulge of TiO₂. The solution of (NiCl₂-FeCl₂), (FeCl₂) or (NiCl₂), were prepared with fixed 5 wt. % for both metal salts and then was released into the TiO₂ suspension. The suspension was agitated for 3 hrs at 300 rpm, at 25°C, and then the slurry was dried at 120°C overnight. The obtained composites (5%

Ni-5% Fe/TiO₂), (5% Ni/TiO₂), and (5% Fe/TiO₂) were marked as Ni-Fe/TiO₂ and Ni/TiO₂, and Fe/TiO₂ respectively.

Characterizations

X-ray diffraction profiles analysis pattern for all the samples was recorded using X-ray Diffractometer Model (JEOL JDX-8030, Tokyo, Japan). The dielectric measurements were carried out by “Solartron frequency and analytical response analyzer instrument for measuring the impedance spectra associated with our samples that were in the form of circular pellets, ~1 mm thick and ~0.5 cm in radius. The pellets were connected in series with small 47 \square resistors to stabilize the signal. The measurement frequency range was $f=0.1$ kHz-0.3 MHz and temperature range 25°C to 150°C with an AC amplitude of 0.3 V at zero DC voltage. The temperature was measured with a T-type thermocouple with its junction just in contact with the sample with accuracy better than ± 1 K.

The composites pellets were prepared as follows: mortar and pestle were used to ground the samples to gain fine powder. The large particles would hinder the pellets to be smooth. Then a small amount of the fine powder sample (0.30 g) was loaded into the hydraulic die-set ket where the pellets being made. The samples were compressed by hydraulic pressure machine at a pressure of 3 tons to make pellets for dielectric measurement. No coating is done on any of the pellets.

Results and Discussion

X-Ray Diffraction (XRD)

The phase composition of the as-synthesized Fe/TiO₂ and Ni-Fe/TiO₂ along with undoped TiO₂ were characterized by XRD, and the typical XRD patterns of each sample are shown in (Figure 1) for 2 θ angle values ranging from 20° to 80°. XRD pattern of TiO₂ peaks shows related to two phases which are anatase and rutile mixed phase.

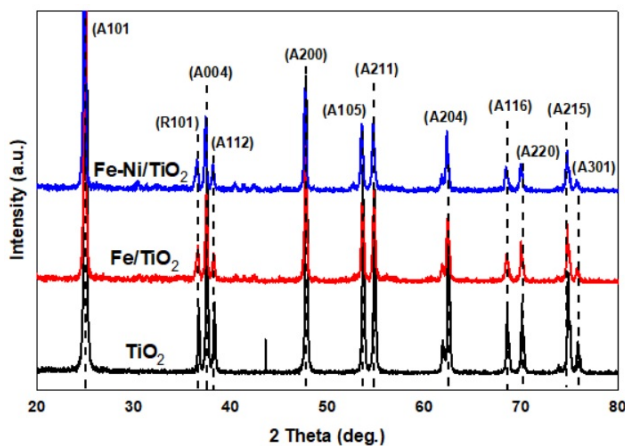


Figure 1: XRD patterns for un-doped TiO₂, Fe/TiO₂, and Ni-Fe/TiO₂.

The Bragg reflections observed at $2\theta=25.3^\circ, 37.2^\circ, 37.69^\circ, 38.35^\circ, 48.03^\circ, 53.83^\circ, 55.01^\circ, 62.8^\circ, 68.8^\circ, 70.4^\circ, 75.2^\circ,$ and 76° , could be assigned to the A101, R101, A004, A112, A200, A105, A211, A204, A116, A220, A215, and A301 diffraction planes, respectively, consistent with standard XRD data for tetragonal phase anatase TiO₂ (crystallographers international tables-JCPDS, no. 21-1272) and literature [16].

Therefore, the XRD spectrum of TiO₂ shows that all diffraction peaks are well indexed to the pure anatase phase except the one present at $2\theta=37.2^\circ$ (101) which demonstrates the occurrence of tetragonal phase rutile TiO₂. No additional peaks other than that for the TiO₂ material were observed indicating impurities free prepared samples within the sensitivity limit of XRD.

For XRD patterns of doped samples, the absence of characteristic iron oxide, nickel oxide, hydroxides and nickel-iron alloy phases indicates that the as synthesized samples have a high degree of crystallinity and Fe and Ni-Fe ions are successfully incorporated into the TiO₂ crystal structure. This is in agreement with other prior studies where no iron was found in the XRD patterns [17,18].

The crystallite size was calculated using the Scherrer equation $D=K\lambda/\beta\cos\theta$; where λ corresponds to the wavelength of Cu $k\alpha$ source (1.5418Å), $K=0.9$ (Scherrer constant), β is the Full Width at Half Maximum (FWHM) for the (101) diffraction peak and θ is the diffraction angle. Values of D around 42, 34 and 32 nm are found for TiO₂, Fe-TiO₂ and Ni-Fe-TiO₂ samples, respectively (Table 1). It is clear that Fe and Ni-Fe doped samples have smaller average crystallite sizes, compared to the undoped TiO₂. The decrease in the mean size with the Fe incorporation is quite expected since the ionic radius of Fe (0.64 Å) is relatively less than that of Ti (0.68 Å). On the other hand, with the entrance of Ni into the Fe-TiO₂ matrix, the size is further decreased showing that Ni may restrain particle agglomeration, forming well-defined nano-crystalline particles, consistent with the reported results of Asiltürk et al. [19] and Khan et al. [20].

The lattice parameters a and c are determined according to the Bragg equation and from the following relation [21], and listed in (Table 1).

Where h, k and l are the Miller Indices, d is inter-planar distance and ‘ a ’ and ‘ c ’ are the lattice parameters. The a lattice constant values calculated for pure and doped TiO₂ were the same (3.81 Å) whereas, the c parameter value was 10.12, 10.16 and 10.23 Å for TiO₂, Fe-TiO₂ and Ni-Fe-TiO₂, respectively, consistent with the reported results of [22]. This suggests that doping induces the decrease of TiO₂ crystallite size along c -axis.

	(D)(nm)	a(Å)	c(Å)	c/a
Pure TiO ₂	40.87	3.81	10.12	2.66
Fe-TiO ₂	36.64	3.81	10.16	2.67
Ni-Fe-TiO ₂	32.22	3.81	10.23	2.69

Table 1: The results of lattice parameters of TiO₂, Fe-TiO₂ and Ni-Fe-TiO₂ samples.

SEM study

To visualize the doping effect on TiO₂ morphology, SEM study was conducted. Figure 2 depicts the SEM images of pure and doped TiO₂ samples.

Pure TiO₂ shows a non-homogeneous spherical particles distribution in form of microstructure agglomerates clusters of different sizes and the nanoparticles are in the size range of ~50 nm-60 nm. It should be noticed that grain distribution was slightly affected by the Fe and Ni incorporation. The Fe-TiO₂ sample consists of agglomerated nanosized primary particles, with size ranging from 40 nm-50 nm, along with pores between the grains. Ni-Fe co-doped

sample has reduced particles agglomeration and gives rise to a granular surface morphology with smaller grain size which is consistent with XRD findings. Therefore, it is possible that Fe and Ni ions can modify the structure of the TiO₂ sample by acting as nucleation sites that support the formation of finer particles.

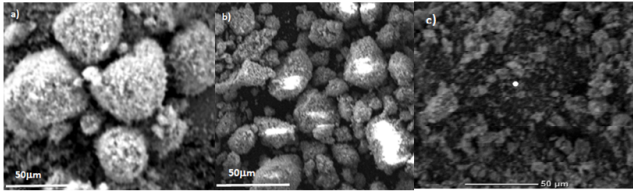


Figure 2: SEM images of a) TiO₂, b) Fe/TiO₂ and c) Ni-Fe/TiO₂ sample.

Dielectric properties

Dependent in frequency: The dielectric permittivity ϵ' ($\epsilon' = Cd/\epsilon_0 A$) as a function of frequency for Fe/TiO₂ and Ni-Fe/TiO₂ at various temperatures is presented in (Figure 3).

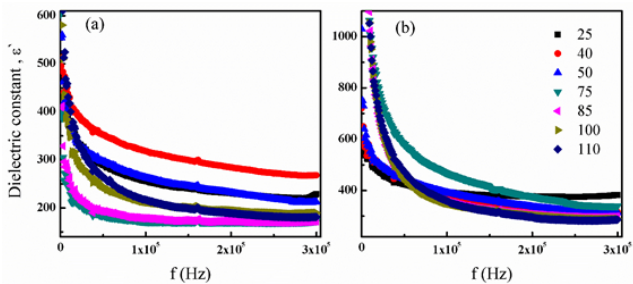


Figure 3: The dielectric permittivity ϵ' versus frequency for (a) Fe/TiO₂ and (b) Ni-Fe/TiO₂, respectively at different temperatures.

It is shown that high dielectric constant in low-frequency range is caused by the Maxwell Wagner-type polarization, the values of ϵ' decreases with increasing frequency altogether samples this may be associated with the decrease in the number of dipoles or the dipoles are no longer able to respond to the electric field [23]. Moreover, the values of ϵ' for Ni-Fe/TiO₂ are relatively higher than those for Fe/TiO₂.

Figure 4 shows the dielectric loss ϵ'' ($\epsilon'' = \epsilon' \tan \delta$) behavior of Fe/TiO₂ and Ni-Fe/TiO₂ at different temperature as a function of frequency. The strong increase in the ϵ'' spectra at low frequencies and high temperatures results from a conduction process obscuring the interfacial polarization which is present in nano-composite samples. The dispersion observed in the low-frequency ϵ'' spectrum is accompanied by an increase in ϵ' . This reveals the formation of space charge regions.

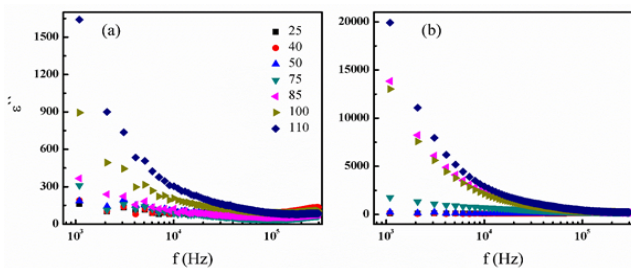


Figure 4: The dielectric loss ϵ'' versus frequency for (a) Fe/TiO₂ and (b) Ni-Fe/TiO₂, respectively at different temperatures.

The dielectric modulus M'' ($M'' = (\epsilon'')/(\epsilon'^2 + \epsilon''^2)$) was studied to avert the contributing of the large value of the dielectric constant and dielectric loss at low frequency related to the Maxwell Wagner-type polarization. Figure 5 shows that the frequency dependence of dielectric modulus for Fe/TiO₂ and Ni-Fe/TiO₂ at different temperatures. It is shown that the zero values of M'' at low temperature indicating the removal of the electrode polarization. Also, ρ relaxation peaks shows at high frequency which attributed to the conductivity current relaxation [24].

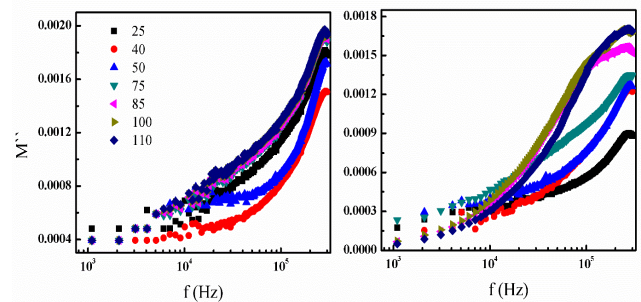


Figure 5: The dielectric modulus M'' versus frequency for (a) Fe/TiO₂ and (b) Ni-Fe/TiO₂, respectively at different temperatures.

The ac conductivity dependent of frequency can be calculated by $\sigma_{ac} = \omega \epsilon_0 \epsilon' \tan \delta$, where ω is the angular frequency, is the permittivity of the free space and $\tan \delta$ is loss tangent. The frequency dependence of σ_{ac} for Fe/TiO₂ and Ni-Fe/TiO₂ composites at different fixed temperatures is shown in Figure 6.

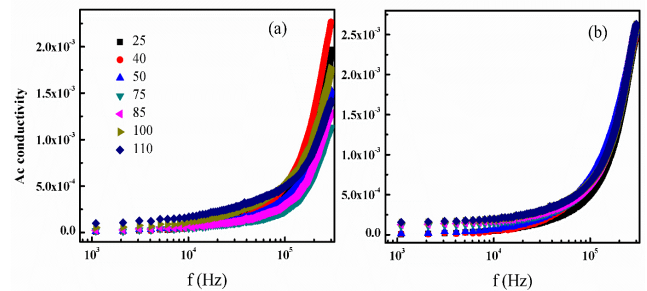


Figure 6: The ac conductivity σ_{ac} versus frequency for (a) Fe/TiO₂ and (b) Ni-Fe/TiO₂, respectively at different temperatures.

For all the samples the ac conductivity increases by increasing frequency which indicates that the most contributing mechanism to explain the action of ac conduction in TiO₂ is the hopping conduction process. The activation energy (E_a) for Fe/TiO₂ and Ni-Fe/TiO₂ composite was calculated by Arrhenius relation $\sigma_{ac} = \sigma_0 \exp(-E_a/kT)$. The ac conductivity ($\ln \sigma_{ac}$) versus ($1000/T$) is illustrated in (Figure 7). Obviously, increases with temperature, this is due to the increase in the absorbed energy which enhances the number of charge carriers in the conduction process. The values of E_a for all investigated samples from $f=5$ kHz to 0.3 MHz are listed in (Table 2). It is shown that the values of E_a are decreased with increasing frequency.

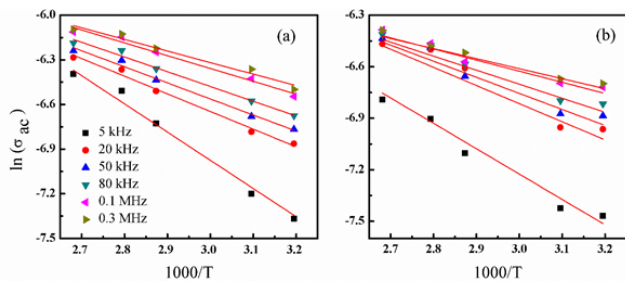


Figure 7: The ac conductivity (\ln) as a function of ($1000/T$) for (a) Fe/TiO₂ and (b) Ni-Fe/TiO₂ respectively at fixed frequencies.

	Frequency	5 kHz	20 kHz	50 kHz	80 kHz	0.1 MHz	0.3 MHz
E _a	Fe/TiO ₂	0.1677	0.1049	0.0956	0.0877	0.0763	0.069
	Ni-Fe/TiO ₂	0.1308	0.0935	0.0829	0.0723	0.0573	0.052

Table 2: Activation energies of Fe/TiO₂ and Ni-Fe/TiO₂ composite according to the Arrhenius relation.

Figure 8 shows the current-voltage (I-V) characteristics of the pure and doped samples. It's clear that the different samples exhibit a linear behavior of the I-V response in the voltage range 0-3 V showing that the contact was ohmic. Fe and Ni doping induces new energy levels in TiO₂ which lower the conduction band edge and result in more electron excitation from the valence band to the conduction band and help them tunneling through the barrier. Ni/TiO₂ system revealed the lowest resistance among all samples proving the formation of an excellent ohmic behavior which can explain the lower resistance conferred to Ni-Fe co-doped system in comparison to Fe doped TiO₂.

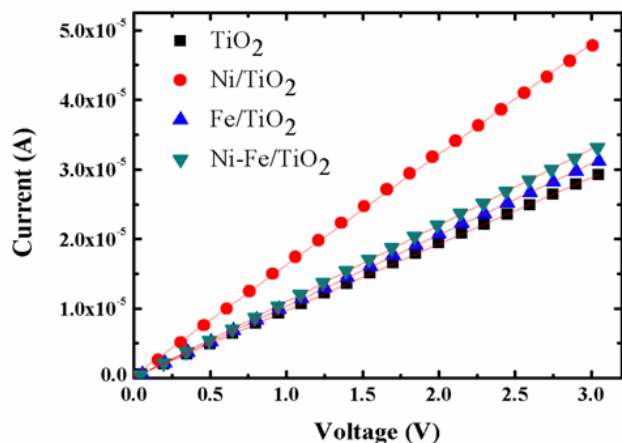


Figure 8: Current-voltage characterization of Fe/TiO₂, Ni/TiO₂ and Ni-Fe/TiO samples.

Conclusion

Based on the characterization results, pure and doped TiO₂ nanoparticles were successfully synthesized by incipient wet

impregnation method. A nano-crystalline anatase sample with average particle size of about 40 nm was confirmed by X-ray diffraction pattern, in good agreement with SEM micrographs which also showed a uniform morphology of nearly spherical nanoparticles.

The dielectric properties for Fe/TiO₂ and Ni-Fe/TiO₂ composite as a function of temperature and frequency were studied. The values of dielectric constant and dielectric loss decrease with increasing frequency. The values of dielectric permittivity for Fe/TiO₂ exhibit relatively lower dielectric constant than Ni-Fe/TiO₂. A relaxation peak has been recognized and shifted to higher frequency with increasing temperature. The ac conductivity increased with frequency which could be related to the hopping conduction process. The values of activation energy E_a for Fe/TiO₂ are higher than Ni-Fe/TiO₂ and decreased with increasing frequency. The high dielectric properties and low activation energy may reflect the importance of Ni-Fe/TiO₂ in dielectric applications.

References

- Jiao L, Guo P, Kong P, Huang X, Li H, et al. (2020) Dielectric properties of (Yb 0.5 Ta 0.5) x Ti 1-x O 2 ceramics with colossal permittivity and low dielectric loss. J Mater Sci Mater Electron 31: 3654-3661.
- Buscaglia MT (2006) High dielectric constant and frozen macroscopic polarization in dense nanocrystalline Ba Ti O 3 ceramics. Phys Rev B 73: 064114.
- Wu J, Nan CW, Lin Y, Deng Y (2002) Giant dielectric permittivity observed in Li and Ti doped NiO. Phys Rev Lett 89: 217601.
- Deepthi K, Pandiyarajan T, Karthikeyan B (2013) Vibrational, giant dielectric and AC conductivity properties of agglomerated CuO nanostructures. J Mater Sci Mater Electron 24: 1045-1051.
- Perumal S, Monikandrabu K, Sambandam CG, Mohamed AP (2014) Synthesis and characterization studies of solvothermally synthesized undoped and Ag-doped TiO₂ nanoparticles using toluene as a solvent. J Eng Res Appl 4: 184-187.
- Priyanka KP, Joseph S, Thankachan S, Mohammed EM, Varghese T (2013) Dielectric properties and AC conductivity of nanocrystalline titanium. J Basic Appl Sci 2: 105-108.
- Sharma R, Sarkar A, Jha R, Sharma AK, Sharma D, et al. (2019) Sol-gel mediated synthesis of TiO₂ nanocrystals: Structural, optical and electrochemical properties. Int J Appl Ceram Technol 17: 1400-1409.
- Wang ST, Sun J, YuY, Li QJ, Tong L, et al. (2018) A facile method to increase dielectric properties of rutile TiO₂. Ceram Int 44: 15110-15115.
- Chao S, Petrovsky V, Dogan F (2010) Effects of sintering temperature on the microstructure and dielectric properties of titanium dioxide ceramics. J Mater Sci 45: 6685-6693.
- Guo B, Liu P, Cui X, Song Y (2018) Colossal permittivity and dielectric relaxations in Tl β Nb co-doped TiO₂ ceramics Ceram Int 44: 12137-12143.
- Wang WY, Zhang D, Xu T, Li X, Zhou T, et al. (2002) Nonlinear electrical behavior and dielectric properties of (Ca, Ta)-doped TiO₂ ceramics. J Alloy Compd 335: 210-215.
- McCormick MA, Slamovich EB (2003) Microstructure development and dielectric properties of hydrothermal BaTiO₃ thin films. J Eur Ceram Soc 23: 2143-2152.

13. Wang Q, Varghese O, Grimes CA, Dickey EC (2007) Grain boundary blocking and segregation effects in yttrium-doped polycrystalline titanium dioxide. *Solid State Ion* 178: 187-194.
14. Hu W, Liu Y, Withers RL, Frankcombe TJ, Noren L, et al. (2013) Electron-pinned defect-dipoles for high-performance colossal permittivity materials. *Nat Mater* 12: 821-826.
15. Bashal AH, Saad MH, Khalafalla MA (2020) The effect of Nickel percentage on the dielectric properties of Bentonite. *J Taibah Univ Sci* 14: 496-499.
16. Wang Y, Li L, Huang X, Li Q, Li G (2015) New insights into fluorinated TiO₂ (brookite, anatase and rutile) nanoparticles as efficient photocatalytic redox catalysts. *RSC Adv* 5: 34302-34313.
17. Li Z, Shen W, He W, Zu X (2008) Effect of Fe-doped TiO₂ nanoparticle derived from modified hydrothermal process on the photo catalytic degradation performance on methylene blue. *J Hazard Mater* 155: 590-594.
18. Mesgari Z, Gharagozlou M, Khosravi A, Gharanjig K (2012) Spectrophotometric studies of visible light induced photo catalytic degradation of methyl orange using phthalocyanine-modified Fe-doped TiO₂ nanocrystals. *Spectrochim Acta A Part A: Mol Biomol Spectrosc* 92: 148-153.
19. Asilturk M, Sayilkan F, Arpac E (2009) Effect of Fe(3+) ion doping to TiO₂ on the photocatalytic degradation of Malachite Green dye under UV and vis-irradiation. *J Photochem Photobiol A Chem* 203: 64-71.
20. Khan MU, Malik RN, Muhammad S (2013) Human health risk from heavy metal via food crops consumption with wastewater irrigation practices in Pakistan. *Chemosphere* 93: 2230-2238.
21. Wilso GJ, Matijasevich AS, Mitchell DR, Schulz JC, Willm GD (2006) Modification of TiO₂ for enhanced surface properties: Finite Ostwald ripening by a microwave hydrothermal process. *Langmuir* 22: 2016-2027
22. Cheng G, Liu X, Song X, Chen X, Dai W, et al. (2020) Visible-light-driven deep oxidation of NO over Fe doped TiO₂ catalyst: Synergic effect of Fe and oxygen vacancies. *Appl Catal B: Environ* 277: 119-196.
23. Hdidar M, Chouikhi S, Fattoum A, Arous M, Kallel A (2018) Influence of TiO₂ rutile doping on the thermal and dielectric properties of nanocomposite films based PVA. *J Alloys Compd* 750: 375-383.
24. Abdel-Baset TA, Hassen A (2016) Dielectric relaxation analysis and Ac conductivity of polyvinyl alcohol/polyacrylonitrile film. *Physica B: Condens Matter* 499: 24-28.